Remote Sensing of Environment 177 (2016) 184–191

Contents lists available at ScienceDirect

Remote Sensing of Environment

journal homepage: www.elsevier.com/locate/rse

Fractional vegetation cover estimation algorithm for Chinese GF-1 wide field view data

Kun Jia [a,*], Shunlin Liang [a,b], Xingfa Gu [c], F. Baret [d], Xiangqin Wei [c], Xiaoxia Wang [a], Yunjun Yao [a], Linqing Yang [a], Yuwei Li [a]

[a] State Key Laboratory of Remote Sensing Science, School of Geography, Beijing Normal University, Beijing 100875, China
[b] Department of Geographical Sciences, University of Maryland, College Park, MD 20742, USA
[c] Institute of Remote Sensing and Digital Earth, Chinese Academy of Sciences, Beijing 100101, China
[d] INRA-EMMAH UMR, 1114 Avignon, France

ARTICLE INFO

Article history:
Received 30 May 2015
Received in revised form 2 February 2016
Accepted 10 February 2016
Available online 26 February 2016

Keywords:
Fractional vegetation cover
GF-1 satellite
Wide field view data
Neural networks

ABSTRACT

Wide field view (WFV) sensor on board the Chinese GF-1, the first satellite of the China High-resolution Earth Observation System, is acquiring multi-spectral data with decametric spatial resolution, high temporal resolution and wide coverage, which are valuable data sources for environment monitoring. The objective of this study is to develop a general and reliable fractional vegetation cover (FVC) estimation algorithm for GF-1 WFV data under various land surface conditions. The algorithm is expected to estimate FVC from GF-1 WFV reflectance data with spatial resolution of 16 m and temporal resolution of four dates. The proposed algorithm is based on training back propagation neural networks (NNs) using PROSPECT + SAIL radiative transfer model simulations for GF-1 WFV canopy reflectance and corresponding FVC values. Green, red and near-infrared bands' reflectances of GF-1 WFV data are the input variables of the NNs, as well as the corresponding FVC is the output variable, and finally 842,400 simulated samples covering various land surface conditions are used for training the NNs. A case study in Weichang County of China, having abundant land cover types, was conducted to validate the performance of the proposed FVC estimation algorithm for GF-1 WFV data. The validation results showed that the proposed algorithm worked effectively and generated reasonable FVC estimates with $R^2 = 0.790$ and root mean square error of 0.073 based on the field survey data. The proposed algorithm can be operated without prior knowledge on the land cover and has the potential for routine production of high quality FVC products using GF-1 WFV surface reflectance data.

1. Introduction

Fractional vegetation cover (FVC), which refers to the fraction of green vegetation seen from the nadir, is an important parameter for characterizing the land surface vegetation conditions (Baret et al., 2013; Gitelson, Kaufman, Stark, & Rundquist, 2002; Jia, Liang, Liu, et al., 2015; Zhang, Liao, Li, & Sun, 2013). FVC is required for many weather prediction models, regional and global climate models, hydrological models and many other land surface models, and has been extensively used in applications of agriculture, soil erosion risk evaluation, drought monitoring, environmental assessment (Gutman & Ignatov, 1998; Matsui, Lakshmi, & Small, 2005; Roujean & Lacaze, 2002; Zhang et al., 2010). Therefore, accurate and timely estimation of FVC on a large scale using high spatial resolution remote sensing data is of great significance for many land surface related applications. For example, water and soil conservation assessments require high spatial and temporal resolution FVC data (Niu, Du, Wang, Zhang, & Chen, 2014), and the rapid FVC estimates from high spatial resolution remote sensing data could be valuable for such similar applications. The Chinese GF-1 is the first satellite of the Major National Science and Technology Project of China, known as the China high-resolution earth observation system. The GF-1 wide field view (WFV) cameras acquire data with high spatial resolution, wide coverage and high revisit frequency (Table 1), which are highly valuable data sources for dynamic monitoring of land surface FVC on a large scale. However, there is limited literature reporting the general algorithm for FVC estimation from GF-1 WFV data. Therefore, exploring the application potential and developing the land surface FVC monitoring methods are urgently needed.

Currently, many FVC estimation algorithms using remote sensing data have been developed, which mainly include empirical methods, pixel unmixing models, and physical model based methods (Baret et al., 2007; Bioucas-Dias et al., 2012; Guerschman et al., 2009; Jiapaer, Chen, & Bao, 2011; Liang, Li, & Wang, 2012; Xiao & Moody, 2005). The empirical methods are based on the statistical relationships between FVC and vegetation indices or reflectance of specific wavebands (Xiao & Moody, 2005). The normalized difference vegetation index (NDVI),

* Corresponding author at: School of Geography, Beijing Normal University, No.19 Xinjiekouwai Street, Haidian, Beijing 100875, China.
E-mail address: jiakun@bnu.edu.cn (K. Jia).

http://dx.doi.org/10.1016/j.rse.2016.02.019
0034-4257/

Table 1
Technical specification of GF-1 WFV cameras.

Payloads	Bands No.	Spectral range (μm)	Spatial resolution	Swath width (km)	Repetition cycle (day)	Local time of descending node
WFV	1	0.45–0.52	16	800 (four cameras combined)	4	10:30 AM
	2	0.52–0.59				
	3	0.63–0.69				
	4	0.77–0.89				

an index calculated from reflectance in the red and near-infrared (NIR) wavebands, is the most frequently used vegetation index for developing empirical FVC estimation models (Jiapaer et al., 2011). Moreover, some other vegetation indices calculated from visible, NIR and short-wave infrared wavebands, such as enhanced vegetation index (EVI), visible atmospherically resistant index (VARI) and modified three-band maximal gradient difference vegetation index (MTGDVI), are also proposed for FVC estimation due to the fact that NDVI may present larger uncertainties in estimating FVC for very dense canopies or open canopies with light or dark bare ground (Gitelson et al., 2002; Jiang, Huete, Didan, & Miura, 2008; Jiapaer et al., 2011). The empirical methods are computationally efficient for large remote sensing datasets and can provide as accurate estimates of FVC in comparison to deterministic or physically based models in regional scales based on the accurate parameterization of the empirical models. However, a large amount of ground measured training samples covering various vegetation types and growth conditions are required for accurately parameterizing the empirical models. In addition, one empirical model is greatly expected to estimate FVC for a specific vegetation type in the specific region, because the quantitative empirical relationship between FVC and vegetation indices or bands' reflectance is varying with vegetation types and regions. For example, Graetz's linear regression model was only suitable for sparse grassland and his nonlinear regression model was specific for degraded grassland (Graetz, Pech, Gentle, & O'Callaghan, 1986). Therefore, though there are some publically available field survey FVC records across most continents (Camacho, Cernicharo, Lacaze, Baret, & Weiss, 2013; Held, Phinn, Soto-Berelov, & Jones, 2015) that can be used to build empirical models, the amount of the records is not enough for accurately parameterizing the empirical models which need samples covering all situations encountered on the Earth's surface. Based on the actual situations, it is costly and not a good choice for developing an empirical FVC estimation algorithm of a specific sensor.

A pixel unmixing model estimates FVC at the sub-pixel level, with the assumption that each pixel is composed of several components and considering the proportion of the vegetation components as the FVC (Jiapaer et al., 2011; Jimenez-Munoz et al., 2009; Phinn, Stanford, Scarth, Murray, & Shyy, 2002). The dimidiate pixel model in the family of pixel unmixing models has been widely used for FVC estimation and has achieved many reliable results at the regional scales (Qi et al., 2000; Wu, Li, Yon, Zhou, & Yan, 2004). For example, GF-1 WFV data are evaluated to estimate FVC using dimidiate pixel model in the Beijing-Tianjin-Hebei region (Zhan et al., 2014). However, a substantial challenge in pixel unmixing model is how to determine endmembers and the spectral response of endmembers because the land surface is very complex, especially for developing the large-scale pixel unmixing model. Therefore, pixel unmixing models are also not optimal for operationally estimating FVC from GF-1 WFV data.

Physical model based methods are based on the inversion of canopy radiative transfer models, which allow to simulate the physical relationships between the vegetation canopy spectral reflectance and FVC (Jia, Liang, Liu, et al., 2015). The physical model based methods establish FVC estimation algorithms that consider more factors and elucidate the physical relationship between remote sensing signal and FVC. Thus, the physical model based methods are widely applicable for FVC estimation in large scale. However, the direct inversion of radiative transfer models is very difficult due to the complexity of the models. Usually, neural networks (NNs) and lookup table methods are the two typical alternative methods for indirect inversion of physical models, and belong to the group of physical model based FVC estimation algorithms. NNs method is based on training datasets simulated by the physical models, and become one of the most important physically based FVC estimation algorithms for their computational efficiency and good performance (Baret et al., 2006; Roujean & Lacaze, 2002). NNs trained over radiative transfer model simulations have been applied with success to estimate FVC from several sensors, leading to several operational FVC production algorithms, such as the POLDER FVC product, which uses NNs and the Kuusk model (Roujean & Lacaze, 2002) and the MERIS and CYCLOPES FVC products, which use NNs and the PROSPECT + SAIL model (Baret et al., 2007; García-Haro, Camacho, & Meliá, 2008). Therefore, based on the reality of work in the field of FVC estimation using remote sensing data, the NN inversion of physical methods is a potentially accurate choice for operationally estimating FVC from GF-1 WFV data.

The objective of this study is to develop a general and reliable FVC estimation algorithm for GF-1 WFV reflectance data under various land surface conditions. The algorithm is expected to operationally produce high quality FVC data from GF-1 WFV surface reflectance data with spatial resolution of 16 m and temporal resolution of four dates. To achieve this objective, we firstly generate a learning dataset using the PROSPECT + SAIL model with large range changes of input parameters to cover various land surface conditions, and then train the NNs for FVC estimation using GF-1 WFV reflectance data. Finally, a case study is conducted to validate the effectiveness of the proposed FVC estimation algorithm for GF-1 WFV data.

2. Methodology

The proposed FVC estimation algorithm for GF-1 WFV data was based on a radiative transfer model inversion. The neural networks approach was selected for the inversion because it was known to be computationally very efficient. Additionally, it was indicated that NNs, when trained over radiative transfer model simulations, could provide accurate surface parameters estimations because of their efficient interpolation capacity (Baret et al., 2007; Fang & Liang, 2005; Leshno, Lin, Pinkus, & Schocken, 1993). Therefore, the FVC estimation algorithm development for GF-1 WFV data consisted of generating a learning dataset using a radiative transfer model, training the NNs, and applying the NNs to estimate FVC from GF-1 WFV data.

2.1. The Chinese GF-1 WFV data

The GF-1 satellite was launched from Jiuquan Satellite Launch Centre (Gansu province, China) in April 2013, and a large amount of data have been obtained since then. GF-1 satellite is in a sun-synchronous orbit at an altitude of 645 km, and carries two panchromatic/multi-spectral (P/MS) and four wide field view (WFV) cameras. The GF-1 WFV sensor observes solar radiation reflected by the Earth in four spectral channels distributed in the visible and NIR spectral domain ranging from 450 to 890 nm. GF-1 WFV data have a spatial resolution of 16 m and swath width of 800 km with four cameras combined, as well as their high frequency revisit time of four days (Wei et al., 2015). The technical specification for GF-1 WFV cameras is shown in Table 1. The high-frequency revisit time, wide coverage ability and decametric spatial resolution of GF-1 WFV data make them highly suitable data sources for dynamic

monitoring of land surface FVC on a large scale. Therefore, development of FVC estimation algorithm for GF-1 WFV data is a significant work.

2.2. Generating the learning dataset

The radiative transfer model was run to simulate actual satellite observations of canopy reflectance based on the relative spectral response profiles of the GF-1 WFV sensor. The widely used SAIL model with hot-spot correction, which assumed the canopy as a turbid medium, was selected because of its ease of use, general robustness, and consistent performance in validation practices (Jacquemoud et al., 2009; Kuusk, 1991; Verhoef, 1984; Verhoef, Jia, Xiao, & Su, 2007). The canopy structure in the SAIL model was characterized by leaf area index (LAI), the average leaf angle inclination (ALA) assuming an ellipsoidal distribution and the hot-spot parameter (Baret et al., 2007). To compute the cover fraction under the assumption of a turbid medium, the classical gap fraction relationship with LAI and ALA was used, and FVC was computed based on the gap fraction from nadir observations. The PROSPECT model was used to simulate the leaf optical properties (Jacquemoud & Baret, 1990). PROSPECT simulated leaf hemispherical transmittance and reflectance using biochemical and biophysical parameters, including the leaf structure parameter (N), leaf chlorophyll a + b concentration (C_{ab}), water content (C_w), carotenoid content (C_{ar}), brown pigment content (C_{brown}) and dry matter content (C_m). The coupled PROSPECT and SAIL model, also referred to as PROSAIL, was then used to simulate the reflectance of vegetation canopies. Because reasonable error of input variables in the radiative transfer model was permitted and did not lead to loss of inversion accuracy, some parameters in the PROSAIL model could be fixed in the simulation (Goel & Strebel, 1983; Qu, Zhang, & Wang, 2012). For the objective of this study was to develop a general FVC estimation algorithm for GF-1 WFV data under various land surface conditions, the input variables for the PROSAIL model (Table 2) were given reasonable ranges to cover different land surface conditions based on previous studies, such as the Leaf Optical Properties Experiment 93 and the algorithms of the CYCLOPYS FVC product (Baret et al., 2007; Hosgood et al., 1990; Jacquemoud et al., 2009; Qu, Wang, Wan, Li, & Zhou, 2008). Therefore, the simulated learning dataset would have representativeness of different land surface conditions.

Reflectance values of soils were also used as input variable for the PROSAIL model. In this study, the soil reflectances were selected from a globally distributed soil spectral library released by the International Soil Reference and Information Centre (access at: http://www.isric.org). The soil reflectances contained various soil types with different properties (Shepherd, Palm, Gachengo, & Vanlauwe, 2003). Therefore, the selection of these soil reflectance data in the PROSAIL model was representative of various soil types. The original soil reflectance in China had 47 sample locations and 245 profiles. To remove data redundancy produced by similar soil reflectances and to avoid a huge calculated amount in the PROSAIL simulation, several representative soil reflectances were determined from the original data. The spectral angle mapper (Dennison, Halligan, & Roberts, 2004; Jia et al., 2011) was selected to evaluate the similarity of different soil reflectances and to further determine several representative soil reflectances used in the PROSAIL model. Considering two spectral vectors with n wavebands, where $X = (x_1, x_2, \ldots, x_n)$ and $Y = (y_1, y_2, \ldots, y_n)$, the spectral angle could be defined as the following:

$$\alpha_{XY} = \cos^{-1}\left[\sum_{i=1}^{n} x_i y_i / [(\sum_{i=1}^{n} x_i^2)^{1/2} (\sum_{i=1}^{n} y_i^2)^{1/2}]\right] \quad (1)$$

where X and Y represent two different soil spectral reflectance vectors, α_{XY} is the spectral angle between the two spectral vectors X and Y, and the value range of α is between 0 and π/2. The two spectral vectors are completely similar when $\alpha = 0$ and completely different when $\alpha = \pi/2$. When the value of α is between 0 and π/2, larger α values indicate greater difference between the two spectral vectors. In this study, soil reflectances with a spectral angle smaller than 0.05 would be considered as similar reflectance and these similar reflectances would be averaged as a representative soil reflectance. Finally, 13 soil reflectances were determined to represent the possible range of soil spectral shapes (Fig. 1).

For any combination of the input variables, top of the canopy reflectance was computed for each wavelength and then resampled to simulate the GF-1 WFV observations using the relative spectral response profiles. A white Gaussian noise with a signal to noise ratio of 100 was added to the simulated reflectances to account for uncertainties in the satellite measurements and models. This simulation finally resulted in 842,400 cases of matched reflectances and FVC values, which were used as the learning dataset for the NNs.

2.3. The neural networks

The NNs learn from a training dataset by mimicking human learning ability to build relationships between variables, which are robust to noisy data and can approximate multivariate non-linear relationships (Ahmad, Kalra, & Stephen, 2010). Currently, NNs have been widely used for estimating land surface variables from remote sensing data (Baret et al., 2013; Jia, Liang, Liu, et al., 2015; Li et al., 2011; Verger, Baret, & Camacho, 2011). Back propagation NNs (BPNNs), a popular type of NNs, simply process nodes arranged into the different layers including input, hidden and output layers. The principle of BPNNs can be described as follows: For determining the output of the NNs for given input data, the BPNNs calculate the difference between the obtained output with the desired output, and then adjust the weights of the synapses to minimize the difference until the overall error is below a

Table 2
The input variables of the PROSAIL model used to generate the training dataset.

Parameters	Units	Value range	Step
LAI	m^2/m^2	0–7	0.5
ALA	°	30–70	10
N	–	1–2	0.5
C_{ab}	μg/cm^2	30–60	10
C_m	g/cm^2	0.005–0.015	0.005
C_{ar}	μg/cm^2	0	–
C_w	cm	0.005–0.015	0.005
C_{brown}	–	0–0.5	0.5
Hot	–	0.1	–
Solar zenith angle	°	25–55	10

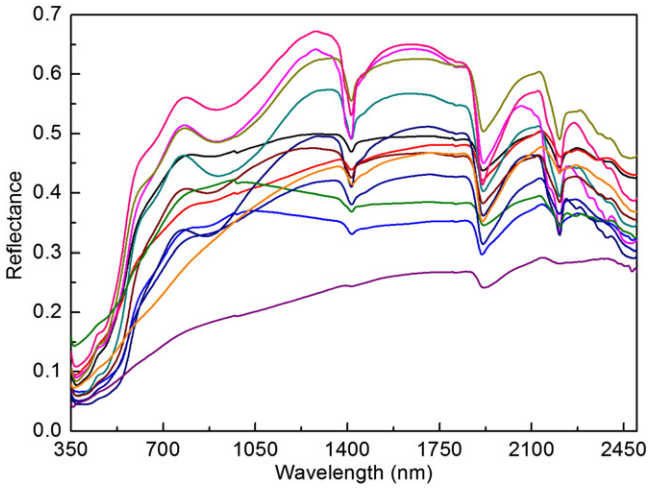

Fig. 1. Reflectance of the 13 soils used to represent the possible range of spectral shapes.

predetermined threshold (Foody, 1999; Jia, Liang, Wei, et al., 2015). BPNNs have been used to estimate essential vegetation variables such as LAI and FAPAR, and proved to be an effective algorithm (Baret et al., 2007). Therefore, BPNNs were selected in this study to build the FVC estimation algorithm for the GF-1 WFV data. The training samples for the BPNNs in this study were derived from the PROSAIL model simulations which modeled the physical relationships between reflectance and FVC with a large ranges of land surface conditions. The BPNNs could learn from the training dataset and built the relationships between reflectance and FVC under different land surface conditions, and then the trained BNPPs could give optimal FVC estimates based on the actual reflectances of remote sensing data. This was the fundamental assumption of using the BPNNs to estimate FVC from the modeled reflectance values under various land surface conditions in this study.

The inputs of the BPNNs included surface reflectance of three GF-1 WFV bands: green (B2), red (B3) and NIR (B4). The blue band (B1) of GF-1 WFV data was not used because the blue band was considered easily contaminated by residual atmospheric effects. The output was the corresponding FVC of the three bands' surface reflectance. The number of nodes in the hidden layer was set to 6. In the BPNNs, the activation functions in the hidden and output nodes were set to "sigmoid" and "linear", respectively. The Levenberg–Marquardt minimization algorithm was used to calibrate the synaptic coefficients because of its efficient convergence capacity (Jia, Liang, Wei, et al., 2015; Ngia & Sjoberg, 2000). The learning dataset made of pairs of inputs and outputs, which were derived from the PROSAIL model simulations, was randomly split into two parts: 90% of the cases were used to train the BPNNs, whereas the rest of the 10% of the cases were used to test the hyperspecialization during the training process. The performance threshold employed mean squared error as the indicator in the training process was set to 0.005. Finally, after 414 iterations, the performance of the training reached the predetermined goal, and the training of BPNNs was completed.

2.4. FVC estimating procedure for GF-1 WFV data

NDVI was usually used to characterize vegetation conditions, distinguish vegetation and non-vegetation regions, and estimate FVC based on a simple linear relationship between FVC and NDVI (Duan et al., 2011; Gutman & Ignatov, 1998; Jiapaer et al., 2011). Therefore, it was a good strategy to remove non-vegetation pixels using an NDVI threshold value before FVC estimation using the NNs, which could avoid the influence of non-vegetation pixels, such as the water body. A conservative NDVI threshold value of 0.05, which was usually used as the bare soil NDVI in the dimidiate pixel model for FVC estimation (Zeng et al., 2000), was selected to identify the non-vegetation pixels. Finally, FVC values in the identified non-vegetation regions would be set to zero, whereas the other regions would be estimated using the trained BPNNs.

3. Case study to validate the proposed algorithm

3.1. Study area and field survey data

A case study was conducted to validate the effectiveness of the proposed FVC estimation algorithm for the GF-1 WFV data. The selected study area was located in Weichang county of Hebei province, China (Fig. 2). The study area is located in the North China region, in the semi-humid and semi-dry climate region of the temperate zone. The annual precipitation is approximately 500 mm, and the annual average temperature is approximately −1.4 to 4.7 °C (Jia, Liang, et al., 2014). A large amount of land cover types are distributed in the study area, which include broad-leaf and coniferous forest, grassland, wetland, cropland, and residential area. Therefore, the complex and abundant land cover compositions are very suitable to validate the FVC estimation algorithm using GF-1 data based on the proposed algorithm.

To acquire the field survey FVC data, a ground survey of detailed vegetation distributions and growth conditions was conducted to select the field measurement sites. Based on the ground survey, 39 sample sites (approximately 30 m × 30 m) were selected in relatively homogeneous regions with approximately 100 m around the sample sites having similar vegetation conditions (Fig. 2). Therefore, the field measurements in the sample sites could match to the pixels of GF-1 WFV data for the validation of FVC estimates from these data. The 39 sample sites contained three potato sites, three corn sites, two wheat sites, eight grass sites, three wetland sites, three grass and shrub mixed sites, thirteen pine sites, three white birch sites, and one pine and white birch mixed site. The center geographic coordinates of each selected site were determined using a handheld global positioning system receiver (Trimble JUNO SB) with a positioning accuracy of approximately ±3 m. The field measurements were performed via digital photography using a Nikon D90 camera from July 24th to 27th, 2014. Within each sample site, usually five survey points were measured with one point at the center of the site and the other four points located at the diagonal of the square. For low vegetation types, the digital images were acquired from the nadir at approximately two meters above the ground at each survey point. Given the tall trees, such as pine and white birch, a bottom-up direction was used to capture the tree canopy, and a top-down direction was used for capturing the low vegetation underneath the tree canopy. The field FVC in the forest regions was determined

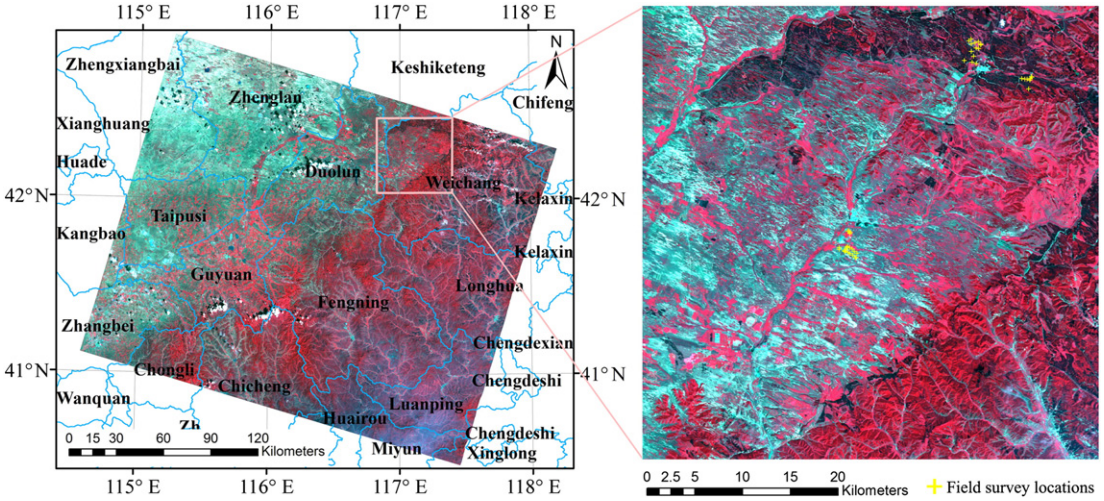

Fig. 2. The geographic location of the study area: the whole scene of GF-1 WFV data (left), the subset study area (right) based on the standard false color composite.

using the following equation that accounts for the FVC of trees and understory vegetation viewed at the nadir direction between tree gaps (Mu et al., 2015):

$$\mathrm{FVC} = f_{\mathrm{up}} + \left(1 - f_{\mathrm{up}}\right) \times f_{\mathrm{down}} \quad (2)$$

where f_{up} and f_{down} are FVC values extracted from the photographs captured by the bottom-up and top-down directions, respectively.

The original digital images were stored in JPEG format, with a size of 4288 by 2848 pixels. To eliminate the distortion from central projection of the digital camera, the edges (40% of the total image length and width, respectively) of the images were cut, resulting in a subset image to represent the survey point. The FVC of each subset image was extracted using an improved method of Gaussian simulation and segmentation method in CIE L*a*b* color space (Liu, Mu, Wang, & Yan, 2012). The improved FVC extraction method introduced hue saturation intensity (HSI) color space to equalize the intensity histogram for enhancing the brightness of shaded parts of the photo, and then the log-normal distribution was used to fit the frequency of vegetation greenness and to classify vegetation and background (Song, Mu, Yan, & Huang, 2015). The improved FVC extraction method was indicated as stable for FVC extraction from the digital images with varying background and shadow conditions. From the results, it could be observed that FVC was effectively extracted for low vegetation types and white birch (Fig. 3). However, FVC extracted for pine trees usually presented lower values than the actual conditions, which was mainly caused by the interruption of arborous branches and dark leaves not being identified. Therefore, the automatic FVC extraction method was not suitable for pine trees. Instead, the maximum likelihood classifier (Duda & Hart, 1973) was used to classify vegetation and background, and then obtain accurate FVC from the photos of pine trees. The classification

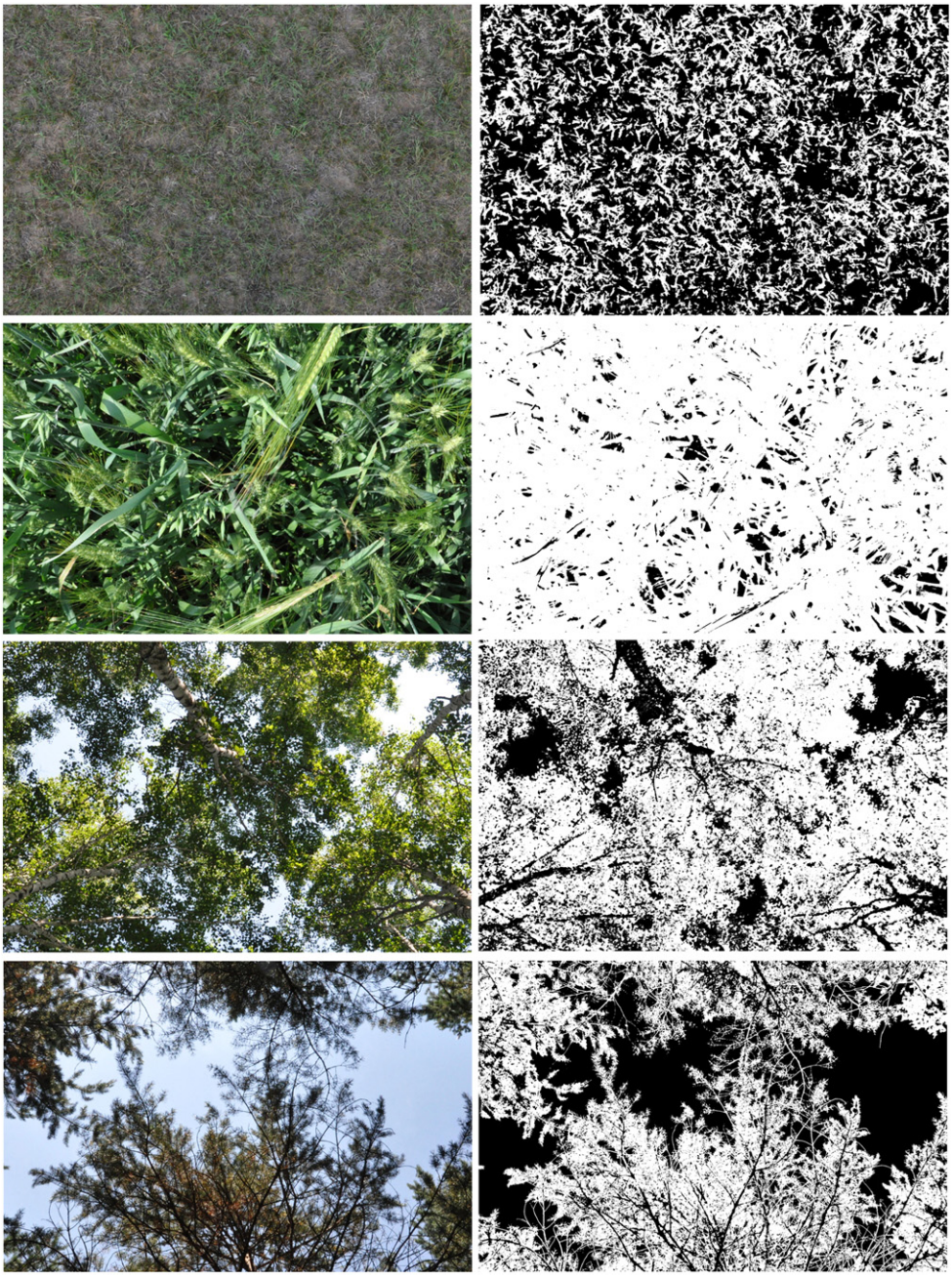

Fig. 3. Examples for determination of FVC from camera images. The left pictures are original camera images, and the right pictures are the corresponding segmentation results.

results were visually satisfactory for FVC extraction in the pine tree sites (the bottom picture of Fig. 3).

3.2. Remote sensing data and preprocessing

GF-1 WFV multispectral data from the fourth camera covering the study area were obtained on July 27th, 2014, which were synchronous with the ground survey period. The image showed little cloud coverage whereas over the study area was cloudless, and the quality of the multispectral data was good (Fig. 2). The GF-1 WFV data were released in the form of a multi-band digital number (DN) grid. Preprocessing of the GF-1 WFV data included radiance calibration, atmospheric correction, and geometric correction. The radiance calibration was to convert the DN value of the raw image to surface spectral reflectance. First, the DN value was converted to radiance using the following equation:

$$Le = Gain * DN + Offset \quad (3)$$

where Le is the radiance, and Gain and Offset are the calibration coefficients obtained from the China Centre for Resources Satellite Data and Application (CRESDA).

The atmospheric correction of GF-1 WFV data was conducted using the Fast Line-of-sight Atmospheric Analysis of Spectral Hypercubes (FLAASH) algorithm. FLAASH was developed to provide accurate, physically-based derivation of atmospheric properties, which was derived from MODTRAN4, to incorporate those same quantities into a correction matrix, and finally to invert 'radiance-at-detector' measurements into the 'reflectance-at-surface' values (Cooley et al., 2002). For the geometric corrections, four Landsat-8 Operational Land Imager data (Jia, Wei, et al., 2014) with high quality, acquired in July and August of 2014, were selected as the base map. The Landsat data had good consistency with the field GPS values, and thus, the geometric correction would be more helpful for locating the field sites with the geometric corrected GF-1 WFV data. The geometric correction was conducted in the environment of Erdas software, and a two-order polynomial transformation with bilinear interpolation was used in the resampling. Finally, 33 ground control points were manually selected from the images, and the resultant geometric co-registration error was less than one pixel of the Landsat data (30 m). To avoid the influence of clouds and a large calculated amount, a subset image consisting of 2986 × 2966 pixels, which covered the area of interest, were extracted from the GF-1 WFV data with World Geodetic System 84 (WGS-84) projection and 16 m spatial resolution (Fig. 2).

3.3. Assessment of FVC estimates using GF-1 WFV data

FVC estimation results using the proposed algorithm and the preprocessed GF-1 WFV data are shown in Fig. 4. In the visual aspect, the high FVC values are distributed in the forest and cropland regions, whereas low FVC values are located in the grassland regions. The spatial distribution of FVC estimates is reasonable. NDVI is an important indicator for FVC conditions because FVC and NDVI display a linear relationship in the dimidiate pixel model for FVC estimation (Jiapaer et al., 2011); thus, the relationship between FVC and NDVI is used to remove inconsistent samples in generating the training dataset used for developing the GEOV1 FVC product algorithm (Baret et al., 2013). Therefore, the strong relationship between FVC and NDVI is a reliable indirect validation indicator of the FVC estimation algorithm at a small regional scale. Thus, the NDVI values calculated from bands three and four of GF-1 WFV data are also shown in Fig. 4 to indirectly validate the performance of the proposed FVC estimation algorithm. It is clearly observed that there is high spatial consistency between the estimated FVC and NDVI values (Fig. 4). The density scatter plots are also shown to present a detailed relationship between the estimated FVC and NDVI in the study area (Fig. 4). A strong relationship between the estimated FVC and NDVI values is observed, except for only a very small amount of pixels. Because a linear regression between FVC and NDVI used for FVC estimation at a regional scale could achieve high quality FVC estimates, the comparison between the estimated FVC and NDVI could indicate that the proposed FVC estimation algorithm for GF-1 WFV data is reasonable and reliable.

Direct comparison using field survey data was carried out to evaluate the performance of the proposed FVC estimation algorithm for GF-1 WFV data. The scatter plots of the estimated FVC and those calculated from the field photos in the ground survey sites are shown in Fig. 5. The overall performance ($R^2 = 0.790$, RMSE = 0.073) using all the field data is presented a satisfactory FVC estimation result which further confirms the reasonability and reliability of the proposed algorithm. The estimated FVC values using the proposed algorithm in the pine sites are concentrated between 70% and 85% (Fig. 5). This is a reasonable distribution because the pines are planted forests in the study area, which have similar forest canopy structures. As for the potato and corn sites, they are in the growth peak period and have very high FVC. These characteristics of potato and corn are presented in the estimated FVC, which are all approximately 90%. The leaves of grass are always threadlike in the study area and the FVC of these grass sites are usually not high. Therefore, the FVC estimates using the proposed algorithm are also reasonable for grassland. In addition, the error in geometrical registration between the field survey location and the remote sensing data pixel is another factor leading to the little differences between the estimated and field FVC.

Thus, in the case of not considering the uncertainty of FVC calculation using the field photos and excluding the errors derived from the geometrical registration, almost all of the difference values between the estimated and field FVC values are within ±10%. To assess the performance of the proposed algorithm from another aspect, the NDVI values in the field survey sites are also extracted and plotted against the estimated FVC (Fig. 5). A clear linear relationship ($R^2 = 0.978$) between the estimated FVC and NDVI is observed for all field survey

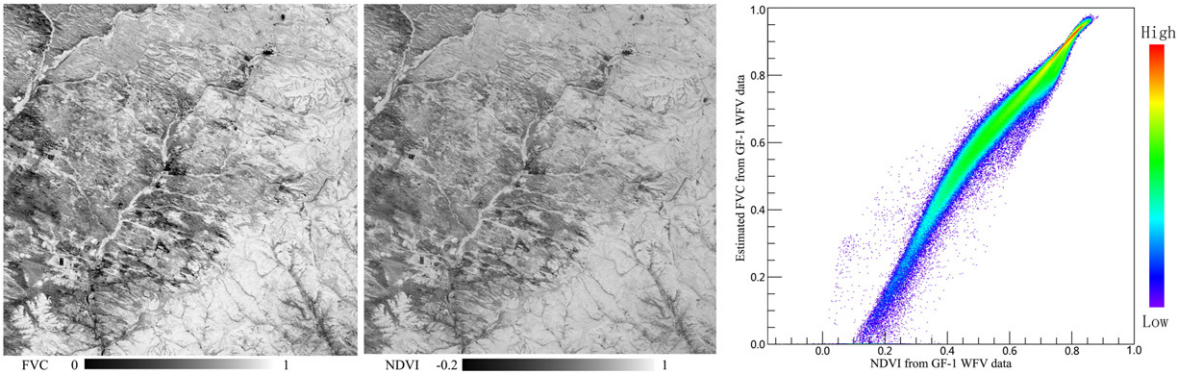

Fig. 4. FVC (left) estimated using the proposed algorithm, NDVI (middle) calculated using the GF-1 WFV data, and the density plots (right) showing the relationship of the estimated FVC and NDVI over the study area.

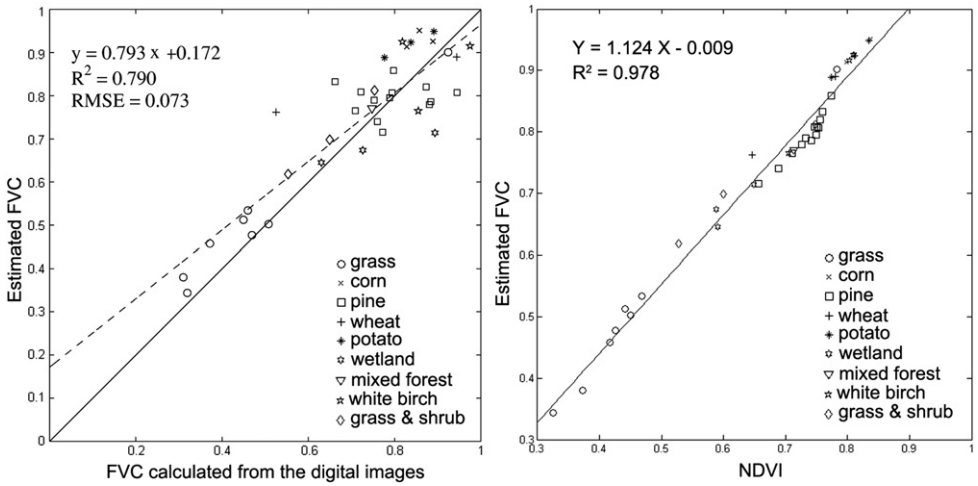

Fig. 5. Comparison of the estimated FVC using the proposed method and that extracted from the field photos (left), and the relationship between the estimated FVC and NDVI (right).

sites. This further indicates that the estimated FVC using the proposed algorithm is reasonable. Therefore, it can be concluded from the above analysis that the proposed FVC estimation algorithm for GF-1 WFV data is reliable and a good choice to be used to routinely produce FVC data from GF-1 WFV surface reflectance data.

4. Discussion and conclusions

This study proposed an algorithm for FVC estimation from GF-1 WFV reflectance data based on training BPNNs with training samples generated from radiative transfer model simulations. The proposed algorithm has achieved satisfactory FVC estimation accuracy compared to the field survey values and has the potential to operationally estimate FVC from GF-1 WFV surface reflectance data. It is automatically operated without any prior knowledge on the land cover, and no human interaction and empirically obtained parameters are required. Therefore, this method could overcome the difficulties in determining the parameters in the empirical method and pixel unmixing models for FVC estimation, which are usually varied with vegetation types and regions. In addition, previous studies on FVC estimation employing NNs based physical methods were mainly focus on kilometric resolution remote sensing data and several kilometric resolution FVC products were generated from SPOT-VET, MERIS, MODIS and AVHRR sensors. This study developed NNs based physical method for FVC estimation from decametric resolution data was a new try, and FVC from decametric spatial resolution data would be better suited for applications related to agriculture, ecosystem and environment management compared to kilometric resolution data which were usually larger than the typical scales of most landscapes.

Furthermore, NDVI was usually strongly related with FVC at a small regional scale and used in empirical methods and dimidiate pixel models for small regional FVC estimates with high accuracies (Jiapaer et al., 2011; Zhang et al., 2013). Therefore, if the estimated FVC had a strong relationship with NDVI at a small regional scale, it could indicate that the FVC estimations were reasonable and indirectly confirmed the proposed method could achieve comparable performance with the empirical methods using NDVI. However, the quantitative relationship between FVC and NDVI was varied with different regions and conditions, leading to the necessity of developing operational FVC estimation methods, which was not so sensitive to vegetation types and backgrounds, instead of empirical methods using NDVI. In this study, the estimated FVC using the proposed algorithm and GF-1 WFV surface reflectance data presented a strong relationship with the NDVI values which indirectly indicated the reasonability and reliability of the proposed method. In the case study, the atmospheric and geometric correction of GF-1 WFV data is completed manually. If the automatic preprocess approach of GF-1 WFV data being developed, this will form a streamlined FVC estimation workflow from the original released GF-1 WFV DN values, which will make the FVC estimation much simpler and accelerate GF-1 FVC product generation.

The accuracy assessment of the land surface parameters estimation algorithm is another important issue, which is difficult to achieve because of the difficulties in obtaining actual FVC from field surveys. Taking photos from the vertical direction is considered as the optimal method for FVC extraction in field surveys. However, using a bottom-up direction to estimate tree FVC is not advisable, especially for dense tree canopies, because the upper leaves are usually shielded by branches and trunks, which would lead to underestimation of the actual FVC. Perhaps using an unmanned aircraft system flying in the lower altitude is a suitable choice for taking photos from the nadir and extracting FVC of tall vegetation types. Another important issue is how to automatically extract FVC from the photos of coniferous forest types because the needle leaves are inclined to be dark in the photos and not easily identified, which would also lead to underestimation of the actual FVC. Supervised classification methods are efficient for FVC extraction from photos of coniferous forest types, but involving a lot of manual works. Therefore, an effective FVC extraction algorithm from field photos still requires improvement. Though the field survey FVC also has many uncertainties, it is still important for assessing FVC estimation algorithms based on remote sensing data, and more effective approaches are expected in the future.

In conclusion, the proposed FVC estimation algorithm for GF-1 data is reliable and suitable for operationally producing FVC data using GF-1 WFV surface reflectance data. Further work will focus on validating the proposed algorithm in many other typical regions with various land cover types using field survey FVC data with less measurement uncertainties.

Acknowledgments

The authors would like to thank the anonymous reviewers and the editor for the constructive comments and suggestions, all of which have led to great improvements in the presentation of this article. We also thank Dr. X. Mu from Beijing Normal University for providing part of the field survey data acquired in the comprehensive remote sensing experiment in Chengde, 2014. This study was partially supported by the National Natural Science Foundation of China (No. 41301353 and 41331173), the National High Technology Research and Development Program of China (No. 2013AA122801), and the Special Foundation for Free Exploration of the State Key Laboratory of Remote Sensing Science (No. 14ZY-06).

References

Ahmad, S., Kalra, A., & Stephen, H. (2010). Estimating soil moisture using remote sensing data: A machine learning approach. *Advances in Water Resources, 33*, 69–80.

Baret, F., Hagolle, O., Geiger, B., Bicheron, P., Miras, B., Huc, M., ... Leroy, M. (2007). LAI, fAPAR and fCover CYCLOPES global products derived from VEGETATION — Part 1: Principles of the algorithm. *Remote Sensing of Environment*, *110*, 275–286.

Baret, F., Morissette, J.T., Fernandes, R.A., Champeaux, J.L., Myneni, R.B., Chen, J., ... Nickeson, J.E. (2006). Evaluation of the representativeness of networks of sites for the global validation and intercomparison of land biophysical products: Proposition of the CEOS-BELMANIP. *IEEE Transactions on Geoscience and Remote Sensing*, *44*, 1794–1803.

Baret, F., Weiss, M., Lacaze, R., Camacho, F., Makhmara, H., Pacholcyzk, P., & Smets, B. (2013). GEOV1: LAI and FAPAR essential climate variables and FCOVER global time series capitalizing over existing products. Part1: Principles of development and production. *Remote Sensing of Environment*, *137*, 299–309.

Bioucas-Dias, J.M., Plaza, A., Dobigeon, N., Parente, M., Du, Q., Gader, P., & Chanussot, J. (2012). Hyperspectral unmixing overview: geometrical, statistical, and sparse regression-based approaches. *IEEE Journal of Selected Topics in Applied Earth Observations and Remote Sensing*, *5*, 354–379.

Camacho, F., Cernicharo, J., Lacaze, R., Baret, F., & Weiss, M. (2013). GEOV1: LAI, FAPAR essential climate variables and FCOVER global time series capitalizing over existing products. Part 2: Validation and intercomparison with reference products. *Remote Sensing of Environment*, *137*, 310–329.

Cooley, T., Anderson, G.P., Felde, G.W., Hoke, M.L., Ratkowski, A.J., Chetwynd, J.H., ... Lewis, P. (2002). FLAASH, a MODTRAN4-based atmospheric correction algorithm, its application and validation. *2002 IEEE International Geoscience and Remote Sensing Symposium & 24th Canadian Symposium on Remote Sensing* (pp. 1414–1418). Toronto, Canada: IEEE Press.

Dennison, P.E., Halligan, K.Q., & Roberts, D.A. (2004). A comparison of error metrics and constraints for multiple endmember spectral mixture analysis and spectral angle mapper. *Remote Sensing of Environment*, *93*, 359–367.

Duan, H., Yan, C., Tsunekawa, A., Song, X., Li, S., & Xie, J. (2011). Assessing vegetation dynamics in the Three-North Shelter Forest region of China using AVHRR NDVI data. *Environmental Earth Sciences*, *64*, 1011–1020.

Duda, R.O., & Hart, P.E. (1973). *Pattern classification and scene analysis*. New York: Wiley.

Fang, H.L., & Liang, S.L. (2005). A hybrid inversion method for mapping leaf area index from MODIS data: Experiments and application to broadleaf and needleleaf canopies. *Remote Sensing of Environment*, *94*, 405–424.

Foody, G.M. (1999). The significance of border training patterns in classification by a feedforward neural network using back propagation learning. *International Journal of Remote Sensing*, *20*, 3549–3562.

García-Haro, F. J., Camacho, F., & Meliá, J. (2008). Inter-comparison of SEVIRI/MSG and MERIS/ENVISAT biophysical products over Europe and Africa. *2nd MERIS/(A)ATSR user workshop, ESA SP-666*. Noordwijk, The Netherlands: ESA Communication Production Office, European Space Agency.

Gitelson, A.A., Kaufman, Y.J., Stark, R., & Rundquist, D. (2002). Novel algorithms for remote estimation of vegetation fraction. *Remote Sensing of Environment*, *80*, 76–87.

Goel, N.S., & Strebel, D.E. (1983). Inversion of vegetation canopy reflectance models for estimating agronomic variables .1. Problem definition and initial results using the suits model. *Remote Sensing of Environment*, *13*, 487–507.

Graetz, R.D., Pech, R.P., Gentle, M.R., & O'Callaghan, F. (1986). The application of Landsat image data to rangeland assessment and monitoring: the development and demonstration of a land image-based resource information system (LIBRIS). *Journal of Arid Environments*, *10*, 53–80.

Guerschman, J.P., Hill, M.J., Renzullo, L.J., Barrett, D.J., Marks, A.S., & Botha, E.J. (2009). Estimating fractional cover of photosynthetic vegetation, non-photosynthetic vegetation and bare soil in the Australian tropical savanna region upscaling the EO-1 Hyperion and MODIS sensors. *Remote Sensing of Environment*, *113*, 928–945.

Gutman, G., & Ignatov, A. (1998). The derivation of the green vegetation fraction from NOAA/AVHRR data for use in numerical weather prediction models. *International Journal of Remote Sensing*, *19*, 1533–1543.

Held, A., Phinn, S., Soto-Berelov, M., & Jones, S. (Eds.). (2015). *AusCover good practice guidelines: A technical handbook supporting calibration and validation activities of remotely sensed data products*. TERN AusCover.

Hosgood, B., Jacquemoud, S., Andreoli, G., Verdebout, J., Pedrini, G., & Schmuck, G. (1990). *Leaf optical properties EXperiment 90 (LOPEX93)*. Brussels, Italy: European Commission, Joint Research Center, Institute for Remote Sensing Applications.

Jacquemoud, S., & Baret, F. (1990). PROSPECT — A model of leaf optical-properties spectra. *Remote Sensing of Environment*, *34*, 75–91.

Jacquemoud, S., Verhoef, W., Baret, F., Bacour, C., Zarco-Tejada, P.J., Asner, G.P., ... Ustin, S.L. (2009). PROSPECT + SAIL models: A review of use for vegetation characterization. *Remote Sensing of Environment*, *113*, S56–S66.

Jia, K., Liang, S., Liu, S., Li, Y., Xiao, Z., Yao, Y., ... Cui, J. (2015a). Global land surface fractional vegetation cover estimation using general regression neural networks from MODIS surface reflectance. *IEEE Transactions on Geoscience and Remote Sensing*, *9*, 4787–4796.

Jia, K., Liang, S., Wei, X.Q., Li, Q., Du, X., Jiang, B., ... Li, Y. (2015b). Fractional forest cover changes in Northeast China from 1982 to 2011 and its relationship with climatic variations. *IEEE Journal of Selected Topics in Applied Earth Observations and Remote Sensing*, *8*, 775–783.

Jia, K., Liang, S., Zhang, L., Wei, X., Yao, Y., & Xie, X. (2014a). Forest cover classification using Landsat ETM+ data and time series MODIS NDVI data. *International Journal of Applied Earth Observation and Geoinformation*, *33*, 32–38.

Jia, K., Wei, X.Q., Gu, X.F., Yao, Y.J., Xie, X.H., & Li, B. (2014b). Land cover classification using Landsat 8 operational land imager data in Beijing, China. *Geocarto International*, *29*, 941–951.

Jia, K., Li, Q., Tian, Y., Wu, B., Zhang, F., & Meng, J. (2011). Accuracy improvement of spectral classification of crop using microwave backscatter data. *Spectroscopy and Spectral Analysis*, *31*, 483–487.

Jiang, Z., Huete, A.R., Didan, K., & Miura, T. (2008). Development of a two-band enhanced vegetation index without a blue band. *Remote Sensing of Environment*, *112*, 3833–3845.

Jiapaer, G., Chen, X., & Bao, A. (2011). A comparison of methods for estimating fractional vegetation cover in arid regions. *Agricultural and Forest Meteorology*, *151*, 1698–1710.

Jimenez-Munoz, J.C., Sobrino, J.A., Plaza, A., Guanter, L., Moreno, J., & Martinez, P. (2009). Comparison between fractional vegetation cover retrievals from vegetation indices and spectral mixture analysis: Case study of PROBA/CHRIS data over an agricultural area. *Sensors*, *9*, 768–793.

Kuusk, A. (1991). The hot spot effect in plant canopy reflectance. In R.B. Myneni, & J. Ross (Eds.), *Photon-vegetation interactions* (pp. 139–159). Berlin Heidelberg: Springer-Verlag.

Leshno, M., Lin, V.Y., Pinkus, A., & Schocken, S. (1993). Multilayer feedforward networks with a nonpolynomial activation function can approximate any function. *Neural Networks*, *6*, 861–867.

Li, Q.Z., Wu, B.F., Jia, K., Dong, Q.H., Eerens, H., & Zhang, M. (2011). Maize acreage estimation using ENVISAT MERIS and CBERS-02B CCD data in the North China Plain. *Computers and Electronics in Agriculture*, *78*, 208–214.

Liang, S., Li, X., & Wang, J. (2012). *Advanced remote sensing: Terrestrial information extraction and applications*. Oxford: Academic Press.

Liu, Y.K., Mu, X.H., Wang, H.X., & Yan, G.J. (2012). A novel method for extracting green fractional vegetation cover from digital images. *Journal of Vegetation Science*, *23*, 406–418.

Matsui, T., Lakshmi, V., & Small, E.E. (2005). The effects of satellite-derived vegetation cover variability on simulated land-atmosphere interactions in the NAMS. *Journal of Climate*, *18*, 21–40.

Mu, X., Huang, S., Ren, H., Yan, G., Song, W., & Ruan, G. (2015). Validating GEOV1 fractional vegetation cover derived from coarse-resolution remote sensing images over croplands. *IEEE Journal of Selected Topics in Applied Earth Observations and Remote Sensing*, *8*, 439–446.

Ngia, L.S.H., & Sjoberg, J. (2000). Efficient training of neural nets for nonlinear adaptive filtering using a recursive Levenberg–Marquardt algorithm. *IEEE Transactions on Signal Processing*, *48*, 1915–1927.

Niu, R.Q., Du, B., Wang, Y., Zhang, L.P., & Chen, T. (2014). Impact of fractional vegetation cover change on soil erosion in Miyun reservoir basin, China. *Environmental Earth Sciences*, *72*, 2741–2749.

Phinn, S., Stanford, M., Scarth, P., Murray, A.T., & Shyy, P.T. (2002). Monitoring the composition of urban environments based on the vegetation-impervious surface-soil (VIS) model by subpixel analysis techniques. *International Journal of Remote Sensing*, *23*, 4131–4153.

Qi, J., Marsett, R.C., Moran, M.S., Goodrich, D.C., Heilman, P., Kerr, Y.H., ... Zhang, X.X. (2000). Spatial and temporal dynamics of vegetation in the San Pedro River basin area. *Agricultural and Forest Meteorology*, *105*, 55–68.

Qu, Y., Wang, J., Wan, H., Li, X., & Zhou, G. (2008). A Bayesian network algorithm for retrieving the characterization of land surface vegetation. *Remote Sensing of Environment*, *112*, 613–622.

Qu, Y.H., Zhang, Y.Z., & Wang, J.D. (2012). A dynamic Bayesian network data fusion algorithm for estimating leaf area index using time-series data from in situ measurement to remote sensing observations. *International Journal of Remote Sensing*, *33*, 1106–1125.

Roujean, J.L., & Lacaze, R. (2002). Global mapping of vegetation parameters from POLDER multiangular measurements for studies of surface-atmosphere interactions: A pragmatic method and its validation. *Journal of Geophysical Research-Atmospheres*, *107*.

Shepherd, K.D., Palm, C.A., Gachengo, C.N., & Vanlauwe, B. (2003). Rapid characterization of organic resource quality for soil and livestock management in tropical agroecosystems using near-infrared spectroscopy. *Agronomy Journal*, *95*, 1314–1322.

Song, W., Mu, X., Yan, G., & Huang, S. (2015). Extracting the green fractional vegetation cover from digital images using a shadow-resistant algorithm (SHAR-LABFVC). *Remote Sensing*, *7*, 10425–10443.

Verger, A., Baret, F., & Camacho, F. (2011). Optimal modalities for radiative transfer-neural network estimation of canopy biophysical characteristics: Evaluation over an agricultural area with CHRIS/PROBA observations. *Remote Sensing of Environment*, *115*, 415–426.

Verhoef, W. (1984). Light-scattering by leaf layers with application to canopy reflectance modeling — the SAIL model. *Remote Sensing of Environment*, *16*, 125–141.

Verhoef, W., Jia, L., Xiao, Q., & Su, Z. (2007). Unified optical-thermal four-stream radiative transfer theory for homogeneous vegetation canopies. *IEEE Transactions on Geoscience and Remote Sensing*, *45*, 1808–1822.

Wei, X.Q., Gu, X.F., Meng, Q., Yu, T., Cheng, T.H., Jia, K., ... Gao, H. (2015). Review of Chinese GF-1 satellite data and its application. In T. Jancsó (Ed.), *IGIT 2015 International Conference* (pp. 161–165). Budapest, Hungary: Nyugat-magyarországi Egyetem Kiadó, Sopron.

Wu, B., Li, M., Yon, C., Zhou, W., & Yan, C. (2004). Developing method of vegetation fraction estimation by remote sensing for soil loss equation: A case in the Upper Basin of Miyun Reservoir. *2004 IEEE International Geoscience and Remote Sensing Symposium* (pp. 4352–4355).

Xiao, J., & Moody, A. (2005). A comparison of methods for estimating fractional green vegetation cover within a desert-to-upland transition zone in central New Mexico, USA. *Remote Sensing of Environment*, *98*, 237–250.

Zeng, X.B., Dickinson, R.E., Walker, A., Shaikh, M., DeFries, R.S., & Qi, J.G. (2000). Derivation and evaluation of global 1-km fractional vegetation cover data for land modeling. *Journal of Applied Meteorology*, *39*, 826–839.

Zhan, Y., Meng, Q., Wang, C., Li, J., Zhou, K., & Li, D. (2014). Fractional vegetation cover estimation over large regions using GF-1 satellite data. *Proceedings of the SPIE*. Bellingham, WA: SPIE (pp. 92604B-92604B-92608, Beijing, China).

Zhang, X., Liao, C., Li, J., & Sun, Q. (2013). Fractional vegetation cover estimation in arid and semi-arid environments using HJ-1 satellite hyperspectral data. *International Journal of Applied Earth Observation and Geoinformation*, *21*, 506–512.

Zhang, X., Wu, B., Ling, F., Zeng, Y., Yan, N., & Yuan, C. (2010). Identification of priority areas for controlling soil erosion. *Catena*, *83*, 76–86.